Vision Research 48 (2008) 1681–1694

Contents lists available at ScienceDirect

Vision Research

journal homepage: www.elsevier.com/locate/visres

Finite schematic eye models and their accuracy to in-vivo data

Ravi C. Bakaraju *, Klaus Ehrmann *, Eric Papas *, Arthur Ho *

Vision Co-Operative Research Centre, Sydney, Australia
Institute for Eye Research, Sydney, Australia
School of Optometry & Vision Sciences, UNSW, Sydney, Australia

ARTICLE INFO

Article history:
Received 19 November 2007
Received in revised form 3 April 2008

Keywords:
Aberrations
Optics of human eye
Ray tracing and peripheral refraction

ABSTRACT

Measurement of ocular wavefront aberration is becoming a popular clinical technique due to recent technical advances and an increasing awareness of its potential for practical application in the fields of surgical and optical refractive correction. In addition, information about the status of peripheral refraction determined from ocular wavefront aberrations is now being used to monitor the progression of myopia and other refractive errors in children, and as a basis for the study of the process of emmetropization. Several finite, anatomically accurate, wide-angled, model eyes have been proposed previously in an effort to produce a schematic eye that accurately reproduces vision under different practical circumstances. This paper compares these models in terms of their wavefront aberration, image quality metrics and peripheral refraction profiles and contrasts these with data from real eyes to assess their relative utility.

1. Introduction

Anatomically close, schematic, model eyes that can reproduce the optical properties of their human counterparts are extremely beneficial. As these models simulate the real world performance of a human eye, they can be used for a range of research and development purposes including ophthalmic lens design, simulation of on-eye contact lens performance, predicting the outcomes of orthokeratology, refractive surgery or IOL implantation and studying the features of optical component systems. Research continues in this area to arrive at a schematic model eye that closely replicates real eye performance in all its various aspects. Several models have appeared over the last century, with levels of complexity ranging from those with reduced or single refracting surfaces, to others that allow refractive index variation within the lens and have conicoidal, rather than spherical, retinal surfaces. Models that can only predict the first order, or Gaussian, properties of an optical system with small apertures and at small field angles are called paraxial schematic model eyes. Here, only foveal or on-axis performance is described, and the most popular model is that of Gullstrand (1909). Based on Listing's work and later modified by Le Grand and El Hage (1980), this is still considered a standard for retrieving Gaussian ocular properties. Other paraxial models that have been proposed include those of Bennett's (1988), Emsley's (1952), Gullstrand and Blaker (1980), Drasdo and Fowler (1974) and Emsley (1952).

While Gullstrand's exact eye model dealt with the variation of lenticular refractive index by incorporating a two-shell structure, recent efforts have been more elaborate (Popiolek-Masajada, 1999). Pomerantzeff et al. (Pomerantzeff, Fish, Govignon, & Schepens, 1971), used a series of shells to mimic the gradient refractive index of the lens, and both Al-Ahdali and El-Messiery (1995), who incorporated 300 such shells, and Liu et al. (Liu et al., 2005) who used 602, have extended this tactic. Taking a mathematical view, Kasprzak (2000) proposed a new approximation for the whole profile of the human crystalline lens involving hyperbolic cosines.

The advent of ray tracing capability through gradient index media has led to shell structured lenses being replaced by gradient refractive indices bounded by two aspheric surfaces. Several such finite, or wide angle, designs have been suggested as offering good predictions for both on, and off, axis aberrations. Those of Escudero-Sanz and Navarro (1999), Kooijman (1983), Liou and Brennan (1997), Lotmar (1971) and Navarro et al. (1985) are the most popular examples under this umbrella with various proposals being made for the specifications of the various surfaces. The off-axis aberrations of the unaccommodated form of Navarro, Santamaria, and Bescos (1985) model were later extensively analyzed by Escudero-Sanz and Navarro (1999).

Thibos and co-worker's (Thibos, Ye, Zhang, & Bradley, 1992) proposal of a simplified, single reduced surface model achieved some measure of success, as it accurately predicted both the spherical and chromatic aberrations of the eye. However, as pointed out several years earlier, the difficulty remains, that any reduced eye approach is limited in terms of its ability to truly represent real world vision since it cannot incorporate the sort of variation in refracting surfaces that occurs naturally (Le Grand & El Hage, 1980). Siedlecki, Kasprzak, and Pierscionek (2004) attempted to address this problem by combining the surface parameters of Koo-

* Corresponding authors. Fax: +61 02 93857401 (R.C. Bakaraju).
E-mail address: r.bakaraju@ier.org.au (R.C. Bakaraju).

0042-6989/$ - see front matter © 2008 Elsevier Ltd. All rights reserved.
doi:10.1016/j.visres.2008.04.009

ijman (1983) with a lens having aspheric surfaces and a specific gradient index. Although they claimed superior image quality and low spherical aberration for their wide angle model, their work does not appear to have gained wide acceptance and is not among the popularly referenced examples in the literature. In an effort to achieve ever more representative behaviour, other models have included accommodative changes for near (Goncharov & Dainty, 2007; Gullstrand, 1909; Le Grand & El Hage, 1980; Navarro et al., 1985), lenticular refractive index changes with age (Goncharov & Dainty, 2007; Norrby, 2005; Popiolek-Masajada & Kasprzak, 2002; Rabbetts, 1998; Smith, Atchison, & Pierscionek, 1992; Zadnik et al., 2003) and changing refractive error in a generic adult model (Atchison, 2006).

In a further refinement, Goncharov and Dainty (2007) incorporated a mathematical representation of a gradient-index (GRIN) lens and were able to reproduce the properties of two well-known schematic eye models, namely Navarro's model (Escudero-Sanz & Navarro, 1999; Navarro et al., 1985) for off-axis aberrations and Thibos's chromatic on-axis model (Thibos et al., 1992).

Impressive though these various developments have been in understanding the optics of average human eyes and assisting the design of visual optics, it is well accepted that their predictions can be substantially inaccurate for individual real eyes. To address this issue, Navarro et al. have recently proposed the production of personalized eye models using data uniquely derived for each individual (Navarro, Gonzalez, & Hernandez-Matamoros, 2006). Although the optimization method they used was efficient and robustly reproduced the total wavefront aberrations of the eyes tested, its ability to reproduce crystalline lens geometry was limited. Also using an individual approach, Rosales and Marcos (2007), working with eyes having intraocular lenses (IOL), found good correspondence with in-vivo data. This supports the suggestion that Navarro et al.'s attempt was restricted by the use of an incorrect lenticular gradient index profile.

During the history of schematic eye development briefly reviewed above, it is apparent that attention has mainly been focused on the first order properties of the system. Rather less emphasis has been placed on the aberration profile and image quality metrics, or the behaviour of peripherally directed light rays. Our purpose in the present work therefore, was to revisit some selected, previously proposed, wide-angle, finite model eyes and describe their aberration profile and image quality metrics in terms of Zernike coefficients. We then wish to compare these data with those from peer-reviewed real world studies to determine their accuracy. Finally we wish to assess the behaviour of peripheral refraction in these model eyes.

2. Methods

The aberration profile and image quality metrics were evaluated for each of the five wide-angled schematic eye models listed in the Appendix using the ZEMAX EE Edition 2007 (Optical design program) at 5 degrees temporal to the posterior pole of the eye, which is presumably the foveal location, a reference wavelength of 589 nanometers and over variable entrance pupil diameters. Macros were written within the Zemax environment to convert the output into a form more easily comparable with that from commonly available clinical aberrometers. Thus, calculation were made for the RMS of spherical, coma like, higher order (HOA) and total wavefront aberrations for pupil diameters of 3, 4 and 6 mm. Peripheral refraction was also calculated out to 40 degrees in each of the temporal, nasal, superior and inferior visual fields using second order Zernike refraction and a 3 mm pupil. The following Zernike orders were used for the root mean square (RMS) calculations: spherical—4th and 6th, coma like—3rd and 5th, higher order—3rd, 4th, 5th and 6th, total—all orders up to 6th, except piston and tilt (Atchison, 2004, 2005). To obtain the refraction values in the peripheral visual field, an elliptical pupil was assumed. Zernike coefficients were converted to off-axis correction using the methods described by Atchison, Scott, and Charman (2003, 2007).

To facilitate comparison between models the following modifications were made prior to performing calculation:

- As the Lotmar and Koijmann specifications did not include coefficients for chromatic dispersion, the Abbe-value for all the ocular media was taken to be 50.23 (Atchison & Smith, 2000). Due to this simplification, chromatic aberration profiles will not be discussed for these two eyes.
- Liou & Brennan's model considers the retinal surface to be flat plane, hence it can only predict on-axis optical performance. They also used a nasal pupil displacement of 0.50 mm. In our work a 12.4 mm curved retina was incorporated to permit wide angle calculation (Atchison & Smith, 2000) and the pupil was undisplaced.
- Atchison (2006) proposed a refractive error dependent myopic model eye with an elliptical retina having two different eccentricities along horizontal and vertical meridians. The retina was also decentered and tilted. In the present work the average value's of Atchison's two conicoids was taken with no tilts or displacements. As we considered only emmetropic eyes, the spherical equivalent refraction was equated to zero.
- It is well known that, aberration estimates of the eyes can be influenced by the direction of ray tracing and especially by the positioning of the reference stop and its size (Atchison & Charman, 2005; Guirao, Williams, & Cox, 2001). Keeping this in view, the surface "pupil" i.e. the plane perpendicular to the optical axis passing through the vertex of the anterior lens, was considered to be the reference stop for all the models and "into the eye" aberrometry technique was used.

For the analysis of chromatic aberration several trials were made to examine the dispersion curve of the ocular media using various alternative sources and numerous procedures. Several mathematical equations have been proposed to describe the dispersion curve (Atchison & Smith, 2000; Bedford & Wyszecki, 1947; Cauchy, 1895; Conrady, 1960; Gullstrand, 1909; Llorente, Diaz-Santana, Lara-Saucedo, & Marcos, 2003; Polack, 1923; Sivak & Mandelman, 1982; Sharma, Kumar, & Ghatak, 1982). In this study, to standardize the work of all the models, dispersion coefficients were refitted using Sellmeier's equation. The reference beam used for the calculations had three wavelengths in visible spectrum i.e. 420, 589 and 760 nm.

Fourier transformation is a mathematical operation to link the point spread function (PSF), modulation transfer function (MTF), phase transfer function (PTF) and optical transfer function (OTF). In this way, the expected retinal image for any visual object can be computed, overcoming the great handicap imposed on clinicians and visual scientists by the natural inaccessibility of the retinal image (Goodman, 1996). To quantify image quality the metrics Strehl ratio, PSF and Fourier transformed MTF were chosen.

3. Model predictions vs experimental data

The Gaussian properties and Seidel aberrations of the models are well described in *Optics of human eye* (Atchison & Smith, 2000), Appendix 3 *Schematic eyes*. Due to the increasingly widespread use of Zernike polynomials as opposed to Seidel aberrations to describe human visual optics we chose to adopt this method in the following descriptions.

3.1. Monochromatic aberrations

Table 1a shows calculated results for spherical, coma like and higher order aberrations for each of the five eye models. For comparison, Table 1b summarizes data for these same aberrations obtained from real eyes as reported in the literature.

Both the Liou & Brennan and Atchison models predict the spherical aberration to be closer to, and slightly lower than, the average population estimate, for a 6 mm pupil, of 0.10–0.15 μm. The remaining models predict almost 2–3 times more than this.

Atchison predicts an extremely low coma value of 0.04 μm, for 6 mm pupil. However, if, as in his original specification, tilt and decentration are included, the model demonstrates an appreciable level of coma, i.e. 0.20 μm. For the other models, coma is predicted to be closer to the mean range of 0.10–0.20 μm. All the models except Liou & Brennan and Atchison predict higher order aberrations close to the average range of 0.20–0.35 μm. Liou & Brennan and Atchison underestimate higher order aberrations by about 50%.

Fig. 1 shows the RMS of spherical aberration, coma, higher order aberrations and total aberrations using the Zernike coefficients for all the model eyes as a function of pupil size. Note that because the normative group contains a mixture of ametropias, while the eye models are uniformly emmetropic, comparison of total RMS aberrations can only be made within the models and not with the real

Table 1a
Summary of spherical, coma like and higher order aberrations from major peer-reviewed articles in the recent past

Year	Author/group	Pupil	C(4,0) & (6,0) RMS Sph	C(3,±1) & (5,±1) RMS Coma	3rd to 6th Ord RMS (HOA)
1999	Calver et al. (1999)	6	0.175 (Mean)	~	~
2001	Porter et al. (2001)	5	0.138 (Mean)	~	~
2002	Thibos et al. (2002)	6	0.120 (Mean)	~	0.500 (Mean)
2002	Artal et al. (2002)	6	0.110 (Mean)	~	~
2003	Wang and Koch (2003)	6	0.128 ± 0.074	0.170 ± 0.089	0.305 ± 0.095
2003	Isabelle et al. (2003)	5	0.048	0.124	~
2003	Cheng et al. (2003)	6	0.084 ± 0.113	~	0.284 ± 0.095
2003	He et al. (2003)	6	0.06 ± 0.22	~	~
2004	Kelly et al. (2004)	6	0.132 ± 0.017	0.084 ± 0.011	~
2004	Cheng et al. (2004)	5	0.084 (Mean)	~	~
2004	Amano et al. (2004)	6	0.175 (Mean)	~	~
2005	Alio et al. (2005)	6	0.160 (Mean)	~	~
2006	Salmon et al. (2006)	6	0.133 ± 0.094	0.192 ± 0.115	0.327 ± 0.130

Table 1b
Summary of spherical, coma like and higher order aberrations calculated for each of five model eyes at 6 mm pupil diameter

Year	Model eye	Pupil	C(4,0) & (6,0)	C(3,±1) (5,±1)	HOA (Upto 6 Ord)
Root mean square values in microns					
1971	Lotmar (1971)	6	0.32	0.21	0.39
1983	Kooijman (1983)	6	0.27	0.18	0.33
1999	Escudero-Sanz and Navarro (1999)	6	0.24	0.20	0.32
1997	Liou and Brennan (1997)	6	0.11	0.07	0.13
2006	Atchison (2006)	6	0.09	0.04	0.10

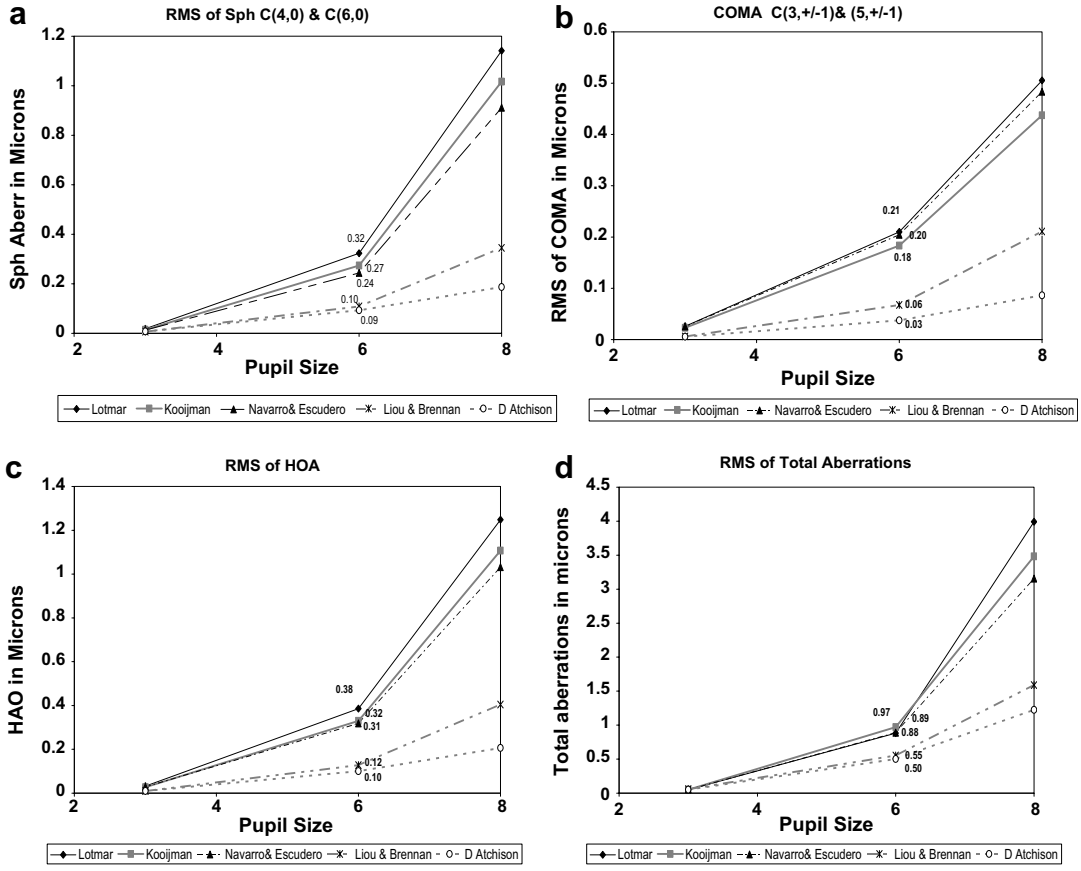

Fig. 1. RMS of spherical aberration (a), COMA (b), higher order aberrations (c) and total aberrations (d) using the Zernike coefficients over variable pupil diameters for all the models.

world outcomes. It is evident that all aberrations of every model converge to zero below a pupil size of 3 mm.

Because spherical aberration plays a significant role in the compensation of corneal aberration by the internal optics of the eye

(Artal, Berrio, Guirao, & Piers, 2002), the contributions of these various components were studied and are listed in Table 2.

Among the model eyes, only Liou-Brennan and Atchison approach real eye behaviour, where the internal optics compensates for the higher corneal spherical aberration. This is probably due to the gradient index profiles defined in these models and perhaps, to a lesser extent, the lenticular curvatures and asphericities chosen. The Goncharov and Dainty model was also similar in this respect. The Lotmar, Kooijman and Navarro-Escudero models predicted corneal and ocular aberrations to be additive in nature.

3.2. Monochromatic aberrations vs eccentricity

It is well known that the optics of the peripheral retina are poor, largely because of defocus together with oblique astigmatism and curvature of field. Only few studies have investigated how aberrations like spherical aberration and coma vary with the retinal eccentricity (Atchison & Scott, 2002; Navarro, Moreno, & Dorronsoro, 1998). Changes of monocular aberrations as a function of eccentric field angle calculated for the models are shown in Tables 3a, 3b and 3c.

As expected, every model predicted increase in aberrations with eccentricity. The RMS of both spherical and higher order aberrations doubled at a retinal eccentricity of 30 degrees, in agreement with previous published data on the off-axis image quality of human eyes (Atchison & Scott, 2002; Navarro et al., 1998). Model predictions also showed that the RMS of coma increased rapidly so that at 30 degrees it was about 6–10 times greater than the central value, a finding not reported in any of the in-vivo studies.

Navarro et al. (1998) found higher mean levels of third-order and fourth order aberrations with changes in visual field and observed substantial asymmetry in all their subjects in that the nasal aberrations were higher than the temporal ones. Clearly, none of the models could have replicated this finding as they all were all rotationally symmetric.

3.3. Peripheral refraction

Atchison et al. have presented a comprehensive investigation into the relationship of peripheral refractive errors in both horizontal and vertical visual fields to the on-axis refraction at different degrees of myopia (Atchison, Pritchard, & Schmid, 2006; Atchison, Pritchard, White, & Griffiths, 2005). We re-calculated the patterns and profiles of peripheral refractive error for the emmetropic population along both horizontal and vertical meridians using the first and second order coefficients provided and compared these with model derived values.

Although emmetropic, the models of Lotmar, Kooijman and Escudero-Navarro predict hypermetropic shifts in the horizontal peripheral field. On the other hand, Liou & Brennan and Atchison predict myopic shifts in the periphery in good agreement with prior experimental studies (Atchison et al., 2006; Atchison et al. 2005; Gustafsson et al., 2001; Millodot, 1981; Seidemann et al., 2002). Even though all the models were configured to simulate an emmetropic eye, most showed a slight myopic shift at the fovea, i.e. zero degrees, for 3 mm pupil. Presumably as a consequence of the assumption of an elliptical conicoid ($Q = 0.26$) for its retina, the Atchison model shows a small shift of the predicted mean sphere (M) towards the hyperopic side at around 30–40 degrees. (See Fig. 2a).

As can be seen in Fig. 2b, the experimental data for the vertical meridian of emmetropes also showed a myopic shift in the periphery. Contrary to that, almost all the models predicted relative hyperopia. Atchison et al. found that emmetropes have a higher relative degree of myopic shift in the vertical meridian than horizontal. In most of the subjects they studied, temporal-nasal asymmetry was observed. However, as none of the models reproduced this, they would appear to share a substantial limitation in this respect.

Table 3a
RMS of spherical aberration with eccentricity (6 mm pupil)

Eccentricity	Lotmar (1971)	Kooijman (1983)	Escudero-Sanz and Navarro (1999)	Liou and Brennan (1997)	D Atchison (2006)
RMS of spherical aberration C(4,0) & C(6,0) in microns					
0	0.33	0.27	0.24	0.11	0.09
10	0.35	0.29	0.27	0.13	0.11
20	0.40	0.32	0.31	0.15	0.13
30	0.42	0.33	0.33	0.18	0.16

Table 3b
RMS of coma with eccentricity (6 mm pupil)

Eccentricity	Lotmar (1971)	Kooijman (1983)	Escudero-Sanz and Navarro (1999)	Liou and Brennan (1997)	D Atchison (2006)
RMS of COMA C(3,±1) & C(5,±1) in microns					
0	0.21	0.18	0.20	0.07	0.04
10	0.63	0.55	0.61	0.19	0.10
20	1.03	0.88	0.99	0.25	0.14
30	1.32	1.12	1.25	0.23	0.10

Table 3c
RMS of HOA with eccentricity (6 mm pupil)

Eccentricity	Lotmar (1971)	Kooijman (1983)	Escudero-Sanz and Navarro (1999)	Liou and Brennan (1997)	D Atchison (2006)
RMS of HOA (3rd to 6th) in microns					
0	0.38	0.32	0.31	0.12	0.10
10	0.72	0.62	0.66	0.22	0.15
20	1.10	0.94	1.03	0.30	0.19
30	1.40	1.18	1.31	0.32	0.22

Table 2
Contribution of corneal and internal optics to the spherical aberration of the human eye

Year	Author/group	P size	Ocular Sph Aberr (Z(4,0))	Corneal (Ant) Sph Aberr (Z(4,0))	Internal Sph Aberr (Z(4,0))
2003	He et al. (2003)	6	0.060	0.300	−0.240
2004	Amano et al. (2004)	6	0.175	0.255	−0.080
2004	Kelly et al. (2004)	6	0.132	0.207	−0.075
2005	Alio et al. (2005)	6	0.160	0.260	−0.100
	Model Eye	P size	Sph Aberr (Z(4,0))	Sph Aberr (Z(4,0))	Sph Aberr (Z(4,0))
1971	Lotmar (1971)	6	0.325	0.166	0.159
1983	Kooijman (1983)	6	0.273	0.190	0.083
1999	Escudero-Sanz and Navarro (1999)	6	0.243	0.189	0.054
1997	Liou and Brennan (1997)	6	0.108	0.239	−0.131
2006	Atchison (2006)	6	0.090	0.260	−0.150

Comparison between mean model eye derived values and the experimental real eye values.

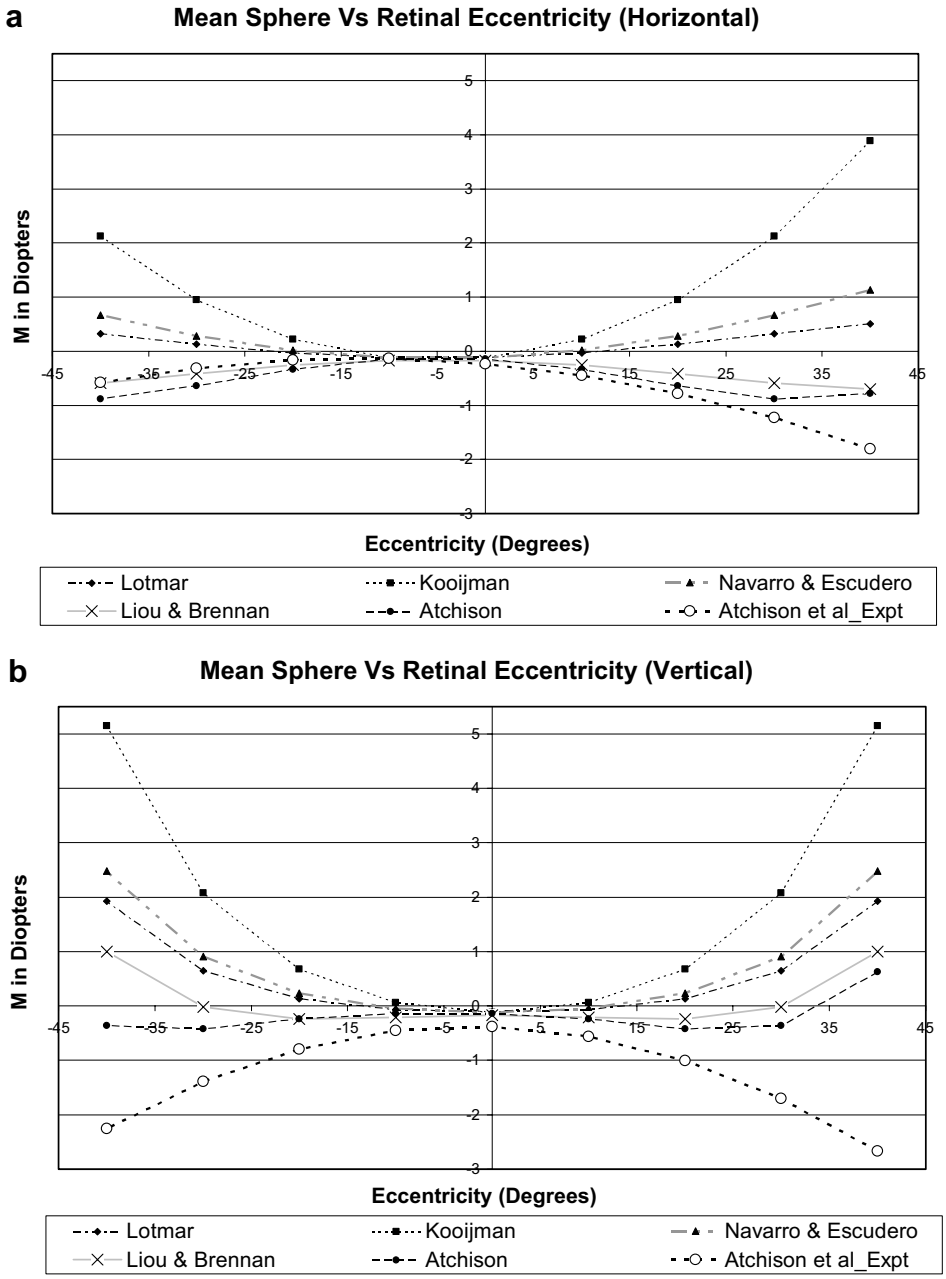

Fig. 2. (a) Mean sphere (*M*) of horizontal peripheral refraction for five schematic models compared to the experimental data reproduced from Atchison et al., 2006. Positive sign indicates temporal retinal meridian, while negative indicates nasal meridian. (b) Mean sphere (*M*) of horizontal peripheral refraction values for five schematic models compared to the experimental data reproduced from Atchison et al., 2006. Positive sign indicates superior retinal meridian, while negative indicates inferior meridian.

The J180 component showed a large amount of astigmatism with increasing eccentricity along the horizontal meridian for all the models. However, the astigmatism predicted by Liou & Brennan and Atchison seems to be overestimated by about 50% compared to both the rest of the models and the experimental data (Atchison et al., 2006). As evident in Fig. 3b, J180 along the vertical visual field showed positive refraction shifts rather than the negative shifts that occurred in the horizontal meridian.

Both Liou & Brennan and Atchison showed similar results along the horizontal and vertical meridians for J180 astigmatism, except that the signs are opposite. Atchison's J180 values were slightly closer to the experimentally derived in-vivo readings, along the vertical meridian. The other four models all returned higher levels of J180 astigmatism, with Kooijman overestimating the J180 values and deviating very substantially from the in-vivo data.

Figs. 4 a and b show J45 as a function of retinal eccentricity for all the models together with data from an experimental in-vivo study (Atchison et al., 2006). Since there is no tilt or decentration of the ocular elements in front of the retina for any of the selected models, the astigmatism (J45) measured in the horizontal periphery always hits zero. However, that was not the case in real eyes (Atchison et al., 2006; Atchison et al., 2005; Gustafsson et al., 2001). Atchison et al. (2006) showed consistent deflections away from zero for the J45 component in the peripheral visual field Most of the values for the vertical meridian were significantly different from zero and were about two to three times greater than those measured horizontally. Along both meridians there were linear relationships between J45 and retinal eccentricity.

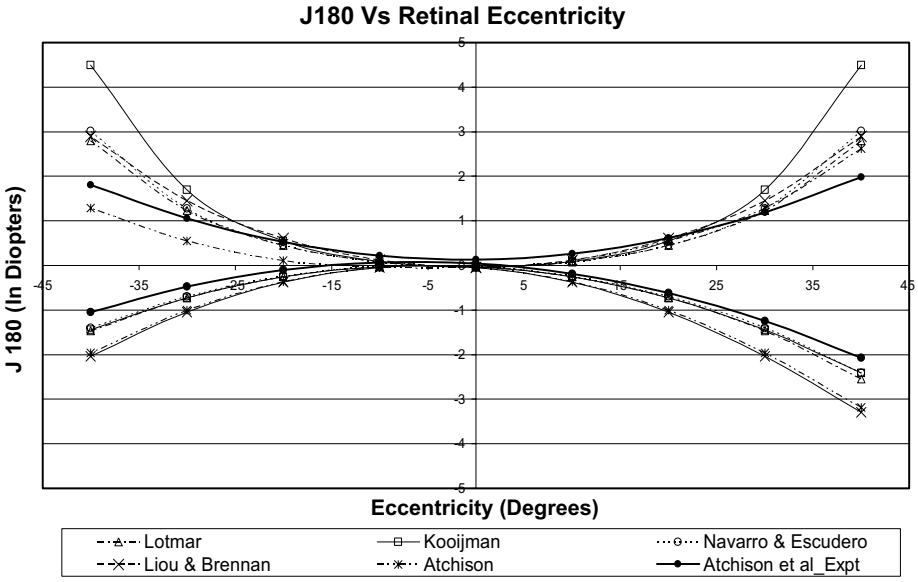

Fig. 3. J180 Astigmatic values of peripheral refraction in both horizontal and vertical meridians. All the schematic eye models compared with experimental data reproduced from Atchison et al., 2006. Data in the positive *Y* direction represent the vertical retinal meridian, while data in the negative *Y* direction represent the horizontal. The positive *X* direction indicates temporal and superior meridians while the negative *X* direction represents nasal and inferior meridians.

3.4. Chromatic aberrations

Chromatic aberration, or dispersion, occurs due to the fact that the refractive index of a material varies with the incident wavelength of light. Refractive power therefore changes for different wavelengths and the system loses the capability of focusing all the wavelengths at a single point.

The chromatic aberration profile for the three relevant models are described in Fig. 5a, b and c, in terms of longitudinal chromatic aberrations and the chromatic focal shift in both millimeters and diopters. While all the results were well within the range limits of the real eye data, Liou & Brennan's model predicted the least on-axis chromatic aberration in the visible spectrum.

Possibly this was due to their assumption that all the ocular media have similar dispersive properties to water a situation contrary actual fact and available experimental evidence (Atchison & Smith, 2000; Bedford & Wyszecki, 1947; Cauchy, 1895 Conrady, 1960; Gullstrand, 1909; Llorente et al., 2003; Mandelman & Sivak, 1983; Sharma et al., 1982; Sivak & Mandelman, 1982).

3.5. Image quality metrics

3.5.1. Strehl ratio

The ratio of the height of the Point spread function curve (PSF) at the Gaussian image point in the presence of aberration, to that of the height of the PSF that would be obtained if no aberration were present (Diffraction Limit), is called the ***Strehl ratio***. This ranges from 0, where significant aberrations are present to 1, for a perfect system. This calculation is valid only for small pupil diameters or optical systems having small wavefront aberrations.

Strehl ratios were calculated for all the models at 3 mm & 4 m pupils, and compared with those of Guirao et al. (1999) who measured the optical performance in subjects aged 20–30 years, with artificial pupils of 3, 4 and 6 mm. The results are shown in Table 4a and it can be seen that all the schematic model eyes predicted a higher ratio than the in-vivo values.

The behaviour of Strehl ratios with retinal eccentricity are shown in Table 4b. At the fovea all the models gave substantially similar results with a mean at 3 mm of 0.7 which falls effectively to zero by 10 degrees off axis.

3.5.2. Point spread function

Point spread function graphs were computed for all the schematic models at a pupil diameter of 6 mm and are shown in Fig. 6. The retinal image qualities retrieved using relative irradiance height and width, were found to be similar in each case.

3.5.3. Modulation transfer function

Modulation transfer function graphs were reproduced from the analytical expressions and constants provided by Artal & Guirao, at a constant pupil diameter and various spatial frequencies (Artal & Navarro, 1994; Guirao et al., 1999). Additional curves were produced using the coefficients given by Navarro & William's group at various retinal eccentricities (Navarro, Artal, & Williams, 1993; Williams, Artal, Navarro, McMahon, & Brainard, 1996). These values were compared to the different schematic model predictions described in Figs. 7 and 8.

Up to a spatial frequency of 60 Cyc/mm, all the schematic models overestimated the MTF compared with experimental in-vivo data. Inspection of Fig. 7 shows a larger area under the Fourier transformed *modulation transfer function* curve, at 6 mm pupil diameter, for both the Liou-Brennan and Atchison models than the rest. However, above 45 Cyc/mm, all the models converged.

Fig. 8, illustrates how the Fourier transformed MTF data of all the models and experimental data as a function of retinal eccentricity, at a 30 Cyc/mm spatial frequency, with 6 mm pupil diameter. The schematic models chosen for comparison predicted off-axis image quality in terms of MTF which declined sharply throughout the retinal field and lapsed to zero in the far periphery of about 40 degree eccentricity.

4. Discussion

We have reviewed various wide-angled schematic model eyes and derived aberrations, image quality metrics and peripheral refraction profiles for each one and compared them with data from peer-reviewed in-vivo studies. Most of our results were consistent with the real eye data (Artal & Navarro, 1994; Atchison et al., 2006; Guirao et al., 1999; Navarro et al., 1993; Navarro et al., 1998), showing that all the models chosen for comparison mimic real world performance reasonably well for small pupil diameters. At

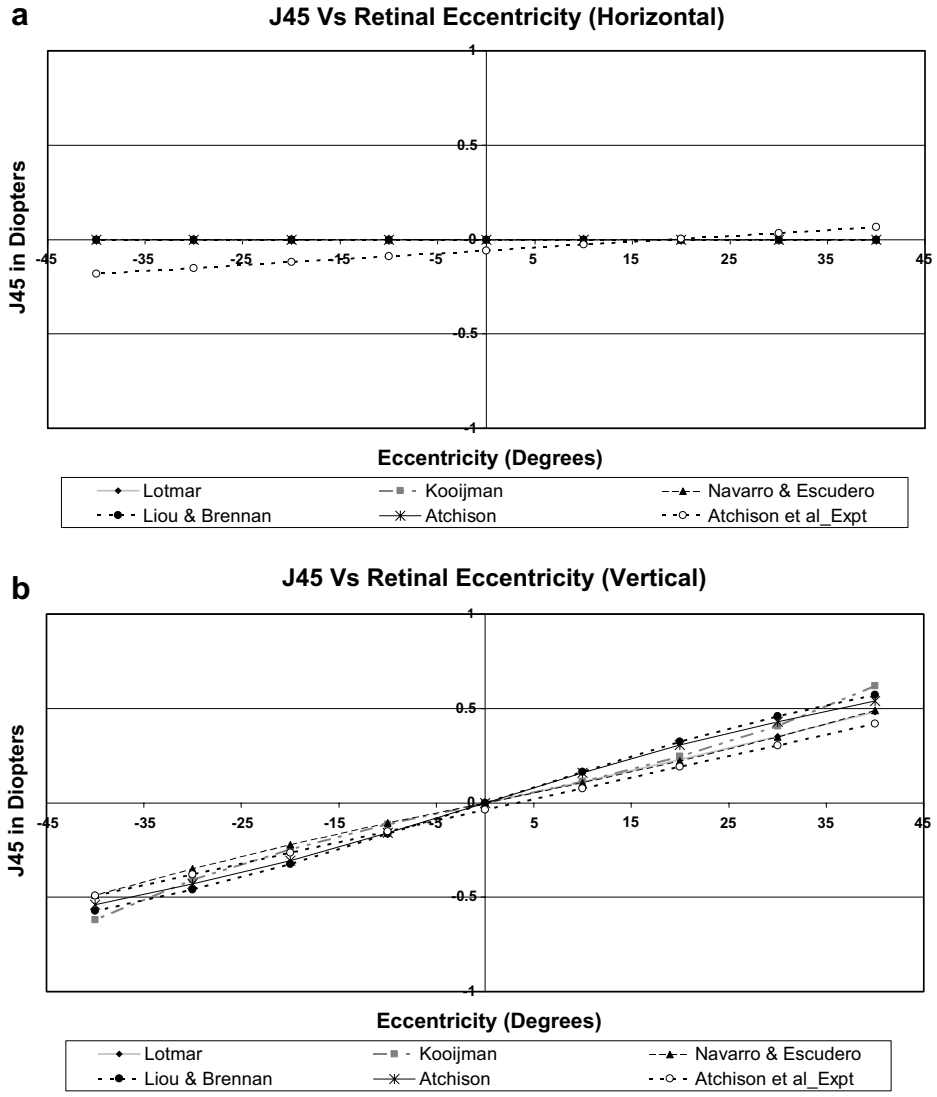

Fig. 4. (a) J45 term of horizontal peripheral refraction values up to 40 degrees of field of all the models compared with experimental data reproduced from Atchison et al., 2006. Positive direction of *X*-axis indicates temporal retina, while negative indicates nasal retinal meridian. (b) J45 term of vertical peripheral refraction values up to 40 degrees of field of all the models compared with experimental data reproduced from Atchison et al., 2006. Positive direction of *X*-axis indicates superior retina, while negative indicates inferior retinal meridian.

large pupil diameters, the Liou-Brennan and Atchison models maintained this good performance; however the others were noticeably less than ideal. Escudero-Navarro's model agrees well with the experimental findings for both on-axis and off–axis aberration properties of the real eye, even though it does not incorporate the gradient index structure of the crystalline lens.

Although in terms of the parameters of the anterior cornea all the models under study were fairly similar several differences were evident in other areas. Probably due to their reliance on Purkinje imaging techniques, which have limited ability to generate acceptable data on the parameters of the posterior corneal surface (Lowe & Clark, 1973), both Lotmar and Escudero-Navarro considered this surface to be perfectly spherical. With the evolution of videokeratoscopy in combination with pachymetry and Scheimpflug imaging techniques, the posterior corneal parameters became better defined (Carney, Mainstone, & Henderson, 1997; Dubbelman, Sicam, & Van der Heijde, 2006; Dubbelman, Weeber, van der Heijde, & Volker-Dieben, 2002; Dunne, Royston, & Barnes, 1992; Eghbali, Yeung, & Maloney, 1995; Patel, Marshall, & Fitzke, 1993; Read, Collins, Carney, & Franklin, 2006). Thus Kooijman, Liou-Brennan & Atchison were able to substitute different levels of prolate asphericity into their models. As a consequence, both the Lotmar and Escudero-Navarro models underestimated the corneal spherical aberration component and had a significant level of coma like aberrations contributed by both corneal and ocular elements. Although the models of Kooijman, Liou-Brennan and Atchison had relatively high amounts of corneal spherical aberration, this was well compensated by the internal optics. The result was low levels of both spherical and coma-like aberrations for the whole ocular system.

The lenticular components of the eye constitute the most debatable parameters of the ocular system, especially the gradient index profile of the lens and the asphericity constants (Q) of both anterior and posterior lenticular surfaces. Most importantly, these play a major role in contributing to the spherical aberration of the whole eye as an imaging system. The Lotmar, Kooijman and Escudero-Navarro models did not incorporate the gradient index profile of the lens. Instead, they considered the lens to have a uniform homogeneous refractive index of 1.42. On the other hand, Liou-Brennan and Atchison fitted the lens refractive index with a gradient index profile based on published data (Atchison & Smith, 1995; Campbell, 1984; Jones, Atchison, Meder, & Pope, 2005; Nakao, Ono, Nag-

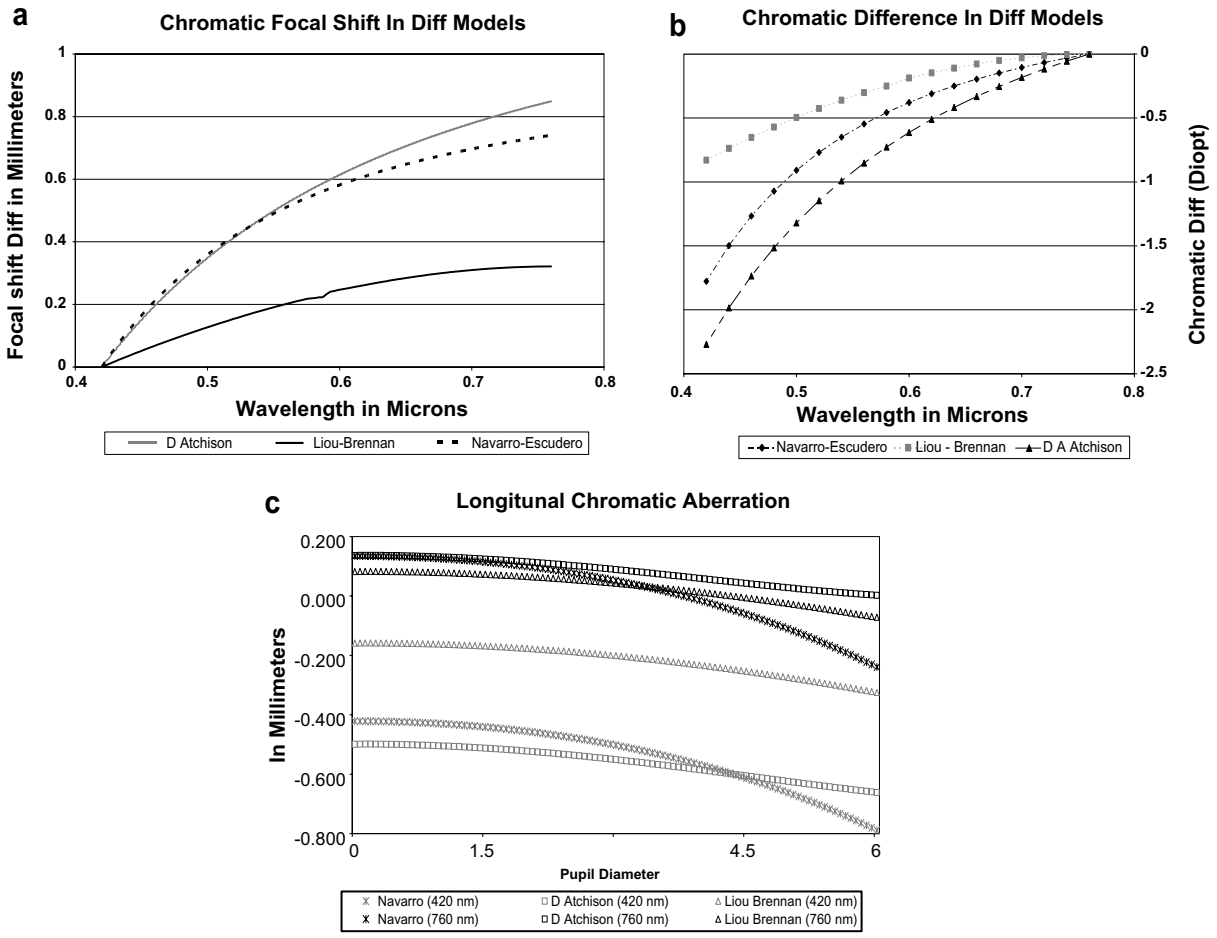

Fig. 5. Chromatic focal shift relative to 420 nm (a) in μm, (b) in dioptres. (c) Longitudinal chromatic aberration.

Table 4a
Strehl ratio values with variation in pupil diameter NC (not computed, due to the limitation of the formula used which is true only for small pupil diameters or optical systems with low wavefront aberrations)

Pupil (mm)	Lotmar (1971)	Kooijman (1983)	Escudero-Sanz and Navarro (1999)	Liou and Brennan (1997)	D Atchison (2006)	Guirao et al. (1999)
Strehl ratio vs pupil diameter						
3	0.797	0.811	0.789	0.703	0.766	0.40
4	0.291	0.303	0.340	0.187	0.215	0.20
6	NC	NC	NC	NC	NC	0.10

Table 4b
Strehl ratio values with variation in retinal eccentricity

Eccentricity	Lotmar (1971)	Kooijman (1983)	Escudero-Sanz and Navarro (1999)	Liou and Brennan (1997)	D Atchison (2006)
Strehl ratio vs peripheral field (3 mm pupil)					
0	0.797	0.811	0.789	0.703	0.766
10	0.239	0.144	0.217	0.165	0.180
20	0.048	0.024	0.043	0.017	0.026

ata & Iwata, 1969; Palmer & Sivak, 1981; Pierscionek, 1989; Sivak & Mandelman, 1982).

For the surface radii and asphericity constants Liou-Brennan relied on Brown's (1974) measurements to derive a symmetric conicoid to represent the shape of both anterior & posterior lens surfaces. Atchison used Dubbelman and colleagues data (Dubbelman & Van der Heijde, 2001; Dubbelman, van der Heijde, & Weeber, 2001) to fit these lens parameters. Being aware of the accumulated effects of errors in ray tracing backwards through the eye in the Scheimpflug technique used by Dubbelman, he felt that the posterior surface asphericity constants were likely to be inaccurate. Accordingly he chose a value that ensured the spherical aberration term of the model was consistent with literature normative data.

It is known that the lenticular parameters, especially the gradient index profile and the asphericity constants, contribute most significantly to the disagreement between models. In an attempt to satisfy both Navarro's monochromatic off-axis and Thibos's chromatic on-axis performance, Goncharov and Dainty (2007) proposed complex mathematical equations to describe gradient index profiles for three different versions, namely unbalanced (U), balanced (B) and simplified (S). They attempted to describe the refractive index distribution in the crystalline lens by using analytical methods that can be easily adapted for age related changes in the shape of the lens and optical power. Adopting 'reverse ray-tracing', otherwise known as the 'eye-inverse' method, they made the anterior and posterior lens asphericity constants variables during an optimization routine, resulting in final coefficients of −1.0 and 0.50, respectively.

Liou-Brennan approach was to derive a gradient index profile from anatomical data (Atchison & Smith, 1995; Brown, 1974; Campbell, 1984; Nakao et al., 1969; Palmer & Sivak, 1981; Pierscionek, 1989; Sivak & Mandelman, 1982). They considered the ante-

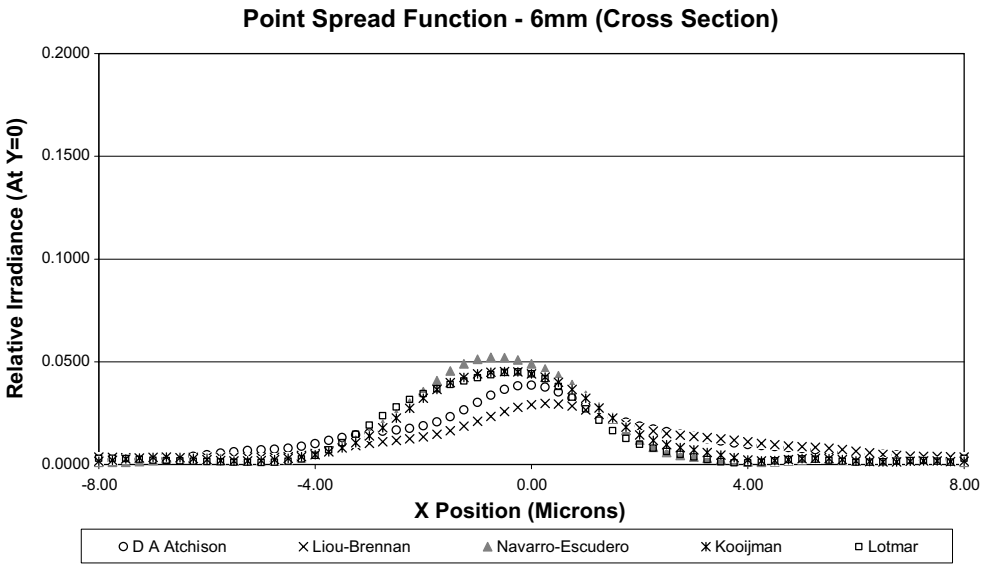

Fig. 6. Point spread function (At 6 mm pupil) for all models.

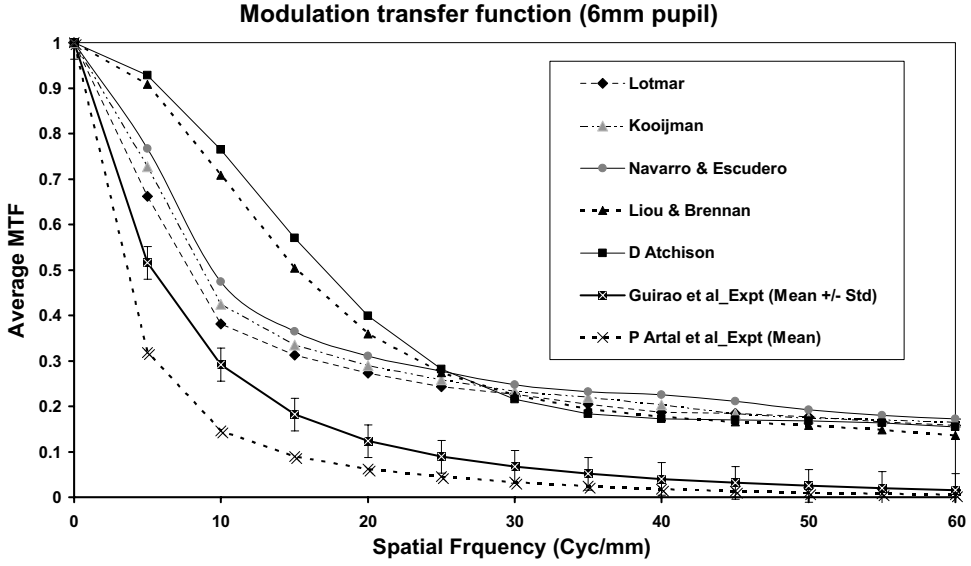

Fig. 7. Fourier transform average MTF for a 6 mm pupil for all the models.

rior lens surface to be a prolate ellipse with $Q = -0.96$, and the posterior lens surface to be an oblate ellipse of $Q = +0.96$. These values appear to depart from the recent in-vivo experimental data of Dubbelman, Van der Heijde, and Weeber (2005); Dubbelman, Van der Heijde, Weeber, and Vrensen (2003).

Exact distribution of refractive index within the human lens though critical for an accurate optical model is still one of the most difficult parameters to measure (Dubbelman & Van der Heijde, 2001; Dubbelman et al., 2001, 2002, 2005; Navarro, Palos, & Gonzalez, 2007a, Navarro, Palos, & Gonzalez, 2007b; Pierscionek, 1988, 1989; Rosales, Dubbelman, Marcos, & van der Heijde, 2006; Smith, Pierscionek, & Atchison, 1991, 1992; Smith, 2003; Smith & Atchison, 2001; Smith & Garner, 1996; Vazquez, Acosta, Smith, & Garner, 2006). Recent advances in instrumentation and technology are creating opportunities to access more reliable normative data on ocular biometrics. One of these (Jones et al., 2005), uses non-invasive magnetic resonance imaging to measure the refractive index distribution, and appears promising as a means of providing more realistic data.

Kooijman offered two models of retinal radii, one with a radius of -10.80 and Q of zero and the other with a radius of -14.10 and Q of 0.36. While on-axis, the aberration profile and refraction performance were similar between the two scenarios, the off axis aberration profile and peripheral refraction differed. Both showed a peripheral hyperopic shift, but the flatter retina was relatively lower and closer to the in-vivo data.

Most of the wide angled models proposed give a reasonably good prediction of spherical aberration on axis. This is not unexpected, as the parameters are deliberately selected to achieve this goal. For example, Atchison chose the posterior surface asphericity to satisfy the condition of optimal spherical aberration to agree with literature values. Goncharov & Dainty chose both the anterior and posterior lenticular asphericities to be variables in the optimization routine, again to satisfy the condition of real eye spherical aberration. This constitutes a reverse ray tracing approach where ocular parameters are adjusted to achieve a specific aberration profile.

Several efforts have been made to calculate modulation transfer function (MTF) of human in-vivo eyes for different pupil sizes and

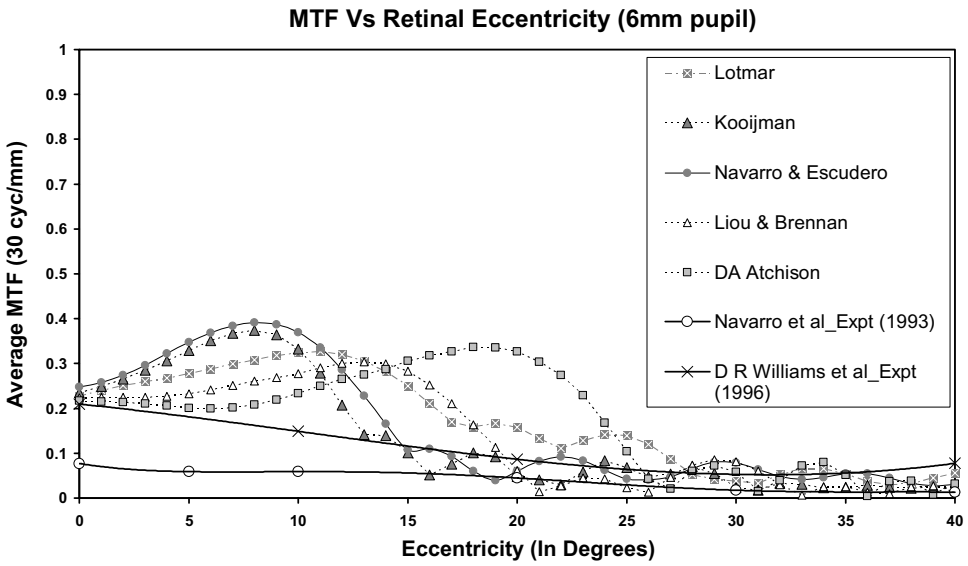

Fig. 8. Fourier transformed average MTF with eccentricity at 6 mm pupil diameter (all models).

retinal eccentricities in various age groups using a double-pass method (Artal, Ferro, Miranda, & Navarro, 1993; Artal & Navarro, 1994; Guirao et al., 1999; Jennings & Charman, 1978, 1981; Liang & Williams, 1997; Navarro et al., 1993; Williams et al., 1996). Navarro et al. (1993), using an improvement on the double pass procedure of Santamaria, Artal, and Bescos (1987), measured the two-dimensional monochromatic modulation transfer function at several field angles in the horizontal meridian of the retina. Their results were in line with the conclusions of Jennings and Charman (1978, 1981) and provided reasonable estimates of the off-axis modulation transfer function. Navarro et al. (1993) used free-state accommodation and natural pupil measurements, while Williams et al. expanded their investigation to obtain measurements at 3 mm pupil with paralyzed accommodation (Williams et al., 1996). Common to all these groups is the rather small sample size they had available.

All the schematic models we studied predicted relatively good off-axis image quality over a wide visual field that declined sharply to near zero levels beyond 40 degrees. These predictions slightly over estimate the image quality when compared to the findings of experimental studies of different groups of researchers (Artal & Navarro, 1994; Navarro et al., 1993; Navarro et al., 1998; Williams et al., 1996). This can be partly attributed to the apodization of pupil and scattering function in the human eye. Apodization refers to the uniformity of illumination in the entrance pupil of an optical system. By default the pupil is always uniformly illuminated in the software used for simulation. Moreover, all schematic modeling assumes a scatter free environment. Clearly, this is not true in the real eye, where image formation is strongly influenced by scattering. Finally, the Stiles-Crawford effect governs the illumination level at retinal eccentricities but was not accounted for (Atchison & Smith, 2000; Drasdo & Fowler, 1974; Stiles & Crawford, 1993).

The theory that defocus and astigmatism induced in the peripheral retina has been credited to influence the development of myopia, and has lead to a large increase in research activities in peripheral refraction. Different peripheral refraction patterns have been reported with various levels of ametropia. Overall these studies suggest that both hypermetropes and emmetropes have relative myopic shifts in the horizontal peripheral field, while myopes have relative hypermetropic shifts (Atchison et al., 2006; Atchison et al., 2005; Charman, 2005; Charman & Jennings, 2006; Gustafsson et al., 2001; Millodot, 1981; Seidemann, Schaeffel, Guirao, Lopez-Gil, & Artal, 2002). Gustafsson et al. found that peripheral refraction in emmetropic in-vivo eyes have large astigmatism, i.e. J180 about 5–8 diopters with increased in retinal eccentricity up to 50 degrees, however with large individual variations. All the models here predicted way less than this dioptric range.

To give further insight we considered how minor amendments to the individual parameters of five models might be made so that their predictions would match real eyes. From discussion above, it is evident that Liou-Brennan & Atchison's models attempt to reproduce real eye performance was reasonably successful. While the remaining three models were fairly close to this, slight changes in their parameters would appear to be able to move them closer still. For example, if the anterior and posterior lenticular asphericities in these models are chosen to be −4 & −2, respectively, both the RMS of spherical and coma like aberrations fall into the real eye range. If retinal curvature is slightly flattened to −13 mm rather than −12 mm for both Lotmar & Escudero-Navarro eyes and the −14 mm radius and a Q of 0.36 taken for Kooijman, peripheral refraction profiles all become similar to those predicted by Liou-Brennan and Atchison models and also are close to the human findings.

The last modification derives from the fact that real eye retina are asymmetrical in that they show different curvature along the horizontal and vertical meridians (Atchison et al., 2004; Mutti, Sholtz, Friedman, & Zadnik, 2000). Re-calculating peripheral refraction for Atchison's model with the two different retinal conicoids that he proposed, gave a closer fit to the in-vivo data especially for the vertical meridian.

It will be remembered that certain modifications were made to the model specifications in order to permit a harmonized approach to calculation. To verify that these changes were relatively inconsequential, we recalculated each model after replacing the original parameters with the following results.

The exercise of replacing the nasal pupil displacement into the Liou-Brennan model calculations, as in their original proposal, did not result in any significant change from the un-displaced version.

In turn, Atchison's model was re-analyzed after replacing tilts to the lens and retina and decentering the latter. For coma like aberrations, the RMS for this model came out to be very large, at about 0.20 μm. With 3 degrees of corneal tilt however, this reverted back into the expected normal range. Peripheral refraction profiles predicted by these tilted models did not well match the data from real eyes.

Over the last 100 years, a large number of optical models of the human eye have evolved with a wide range of sophistication and features. Some have included changes in accommodation for near objects, others incorporated lenticular refractive index changes with age, and few looked into changes with refractive error, still others included tilted and decentered retinal ellipsoids, tilted lens and displaced pupils. The next generation of optical models is expected to be based on the latest results of ocular parameter measurements and to include the use of toroidal corneas, the Zernike description of the whole cornea surface rather than mean keratometric values, and also decentration and tilt of the cornea.

It is well known that aberrations, diffraction, and scatter degrade retinal image quality. The first two have been taken into account in most of the previous models discussed. Light scatter could occur from normal aging, cataract, corneal opacity, the iris, the retina and corrective aids. The next stage of sophistication should be incorporating scattering effects into models that "age" as well as including Stiles-Crawford effect when working off axis.

The chief concern to be addressed in eye modeling is the art of showing diversity between models without sacrificing overall generality. We believe that this could only be effectively achieved with personalized eye models such as have been previously discussed. In spite of many novel and promising, advancements in technology intended to effectively understand the highly complex optical system of the human eye with its multilayered crystalline lens structure, the gradient lenticular refractive index profile and the exact shape of the lenticular surfaces still remain a mystery. We look forward to the availability of more robust techniques and the accumulation of additional normative data that will permit future researchers to solve these problems and develop a personalized optical replica of every tested human eye.

5. Conclusion

Among the five selected models, Liou-Brennan & Atchison models gave a closer match with real eye data, in the aspects of RMS spherical aberrations, HOA & Coma and also peripheral refraction profiles. However with minor modifications, other model predictions fell within the proximity of the in-vivo eye data range. The horizontal peripheral profiles of the models show a closer inclination to real eye profiles than the vertical.

Acknowledgment

This research was supported through a scholarship from the University of New South Wales and the Vision Cooperative Research Centre, Australia.

Appendix. Prescriptions of the wide angle model eyes

SNo	Surface name	Radius of curvature	Medium	Thickness	Conic
A. Lotmar (1971)					
1	Cornea Ant	7.80	1.3771	0.55	−0.286*
2	Cornea post	6.50	1.3374	3.05	0
3	Pupil	Infinity	1.3374	0.00	0
4	Ant lens	10.20	1.4200	4.00	0
5	Post lens	−6.00	1.336	16.59655	−1.00
6	Retina	−12.30			

* Adopted from D Atchison instead of using an equation proposed by Lotmar.

SNo	Surface name	Radius of curvature	Medium	Thickness	Conic
B. Kooijman (1983)					
1	Cornea ant	7.80	1.3771	0.50	−0.25
2	Cornea post	6.50	1.3374	3.05	−0.25
3	Pupil	Infinity	1.3374	0.00	0
4	Ant lens	10.20	1.4200	4.00	−3.06
5	Post lens	−6.00	1.336	16.59655	−1.00
6	Retina	−10.80			

Kooijman offered two models of retinal radii; one with a radius of −10.80 with *Q* of zero and the other with a radius of −14.1 with *Q* of 0.36.

SNo	Surface name	Radius of curvature	Medium	Thickness	Conic
C. Liou and Brennan (1997)					
1	Cornea ant	7.77	1.376	0.55	−0.18
2	Cornea post	6.40	1.3374	3.05	−0.60
3	Pupil	Infinity	1.3374	0.00	0
4	Ant lens	12.40	Grad A	1.59	−0.94
5	Equator	Infinity	Grad P	2.43	0
6	Post lens	−8.10	1.336	16.40398	0.96
7	Retina	−12.40			

Grad A = $1.368 + 0.049057\,\mathbf{Z} - 0.015427\,\mathbf{Z}^2 - 0.001978\,(\mathbf{X}^2 + \mathbf{Y}^2)$.

Grad P = $1.407 - 0.006605\,\mathbf{Z}^2 - 0.001978\,(\mathbf{X}^2 + \mathbf{Y}^2)$.

No retinal radius was provided, however a radius of −12.40 was adopted.

Liou and Brennan assumed that dispersion of all the ocular media is similar to dispersion of water and the dispersion coefficients are described by the following equation.

N(media at λ μm) = N (media at 0.555 μm) + 0.0512 − 0.1455 (λ) + 0.0961(λ)^2

SNo	Medium at 555	A
1	Cornea	1.376
2	Aqueous/Vitr	1.336
3	Lens centre	1.407
4	Lens edge	1.368

SNo	Surface name	Radius of curvature	Medium	Thickness	Conic
D. Escudero-Sanz and Navarro (1999)					
1	Cornea ant	7.72	1.376	0.55	−0.26
2	Cornea post	6.50	1.3374	3.05	0
3	Pupil	Infinity	1.3374	0.00	0
4	Ant lens	10.20	1.4200	4.00	−3.131
5	Post lens	−6.00	1.336	16.40398	−1.00
6	Retina	−12.00			

Adopted from; (Atchison and Smith, 2005) who determined chromatic dispersion for all media using 4-term Cauchy's equation $N(\lambda) = A + B/(\lambda)^2 + C/(\lambda)^4 + D/(\lambda)^6$.

SNo	Medium	A	B	C	D
1	Cornea	1.362017	7.00E−03	−1.02E−09	9.76E−13
2	Aqueous	1.322776	7.41E−03	−1.10E−09	1.04E−14
3	Lens centre	1.404662	6.91E−03	−8.20E−08	9.36E−13
4	Vitreous	1.322781	6.39E−03	−8.51E−08	8.13E−13

SNo	Surface name	Radius of curvature	Medium	Thickness	Conic
E. David Atchison modified (refractive error dependent-emmetropic) (2006)					
1	Cornea ant	7.77	1.376	0.55	−0.15
2	Cornea post	6.40	1.3374	3.15	−0.275
3	Pupil	Infinity	1.3374	0.00	0
4	Ant lens	11.48	Grad A	1.44	−5.00
5	Equator	Infinity	Grad P	2.16	0
6	Post lens	−5.90	1.336	16.28	−2.00
7	Retina	−12.80			0.26

At 555 nm,

Grad A = 1.371 + 0.0652778 $\mathbf{Z}$ − 0.0226659 $\mathbf{Z}^2$ − 0.0020399 ($\mathbf{X}^2 + \mathbf{Y}^2$)

Grad P = 1.418 − 0.0100737 $\mathbf{Z}^2$ − 0.0020399 ($\mathbf{X}^2 + \mathbf{Y}^2$)

D Atchison (2006) model followed; (Atchison & Smith, 2005) who determined chromatic dispersion for all media using 4-term Cauchy's equation

$N(\lambda) = A + B/(\lambda)^2 + C/(\lambda)^4 + D/(\lambda)^6$

SNo	Medium	A	B	C	D
1	Cornea	1.361594	6.01E−03	−6.76E−08	5.91E−13
2	Aqueous	1.323016	6.08E−03	−7.07E−08	6.15E−13
3	Lens-centre	1.401105	6.58E−03	−6.16E−08	5.96E−13
4	Lens-edge	1.354665	6.36E−03	−5.96E−08	5.76E−13
5	Vitreous	1.322357	5.56E−03	−5.82E−08	5.04E−13

References

Alio, J. L., Schimchak, P., Negri, H. P., & Montes-Mico, R. (2005). Crystalline lens optical dysfunction through aging. *Ophthalmology, 112*(11), 2022–2029.

Al-Ahdali, I. H., & El-Messiery, M. A. (1995). Examination of the effect of the fibrous structure of a lens on the optical characteristics of the human eye: A computer-simulated model. *Applied optics, 32*(25), 5738.

Amano, S., Amano, Y., Yamagami, S., Miyai, T., Miyata, K., Samejima, T., et al. (2004). Age-related changes in corneal and ocular higher-order wavefront aberrations. *American Journal of Ophthalmology, 137*(6), 988–992.

Artal, P., Berrio, E., Guirao, A., & Piers, P. (2002). Contribution of the cornea and internal surfaces to the change of ocular aberrations with age. *Journal of the Optical Society of America A, Optics, Image Science, and Vision, 19*(1), 137–143.

Artal, P., Ferro, M., Miranda, I., & Navarro, R. (1993). Effects of aging in retinal image quality. *Journal of the Optical Society of America A, 10*(7), 1656–1662.

Artal, P., & Navarro, R. (1994). Monochromatic modulation transfer function of the human eye for different pupil diameters: An analytical expression. *Journal of the Optical Society of America A, Optics, Image Science, and Vision, 11*(1), 246–249.

Atchison, D. A., & Smith, G. (2000). *Optics of the human eye*. Oxford: Butterworth-Heinemann.

Atchison, D. A. (2004). Recent advances in representation of monochromatic aberrations of human eyes. *Clinical & Experimental Optometry, 87*(3), 138–148.

Atchison, D. A. (2005). Recent advances in representation of monochromatic aberrations of human eyes. *Clinical & Experimental Optometry, 88*(1), 5–27.

Atchison, D. A. (2006). Optical models for human myopic eyes. *Vision Research, 46*(14), 2236–2250.

Atchison, D. A., & Charman, W. N. (2005). Influences of reference plane and direction of measurement on eye aberration measurement. *Journal of the Optical Society of America A, Optics, Image Science, and Vision, 22*(12), 2589–2597.

Atchison, D. A., Pritchard, N., & Schmid, K. L. (2006). Peripheral refraction along the horizontal and vertical visual fields in myopia. *Vision Research, 46*(8–9), 1450–1458.

Atchison, D. A., Pritchard, N., Schmid, K. L., Scott, D. H., Jones, C. E., & Pope, J. M. (2005). Shape of the retinal surface in emmetropia and myopia. *Investigative Ophthalmology & Visual Science, 46*(8), 2698–2707.

Atchison, D. A., Jones, C. E., Schmid, K. L., Pritchard, N., Pope, J. M., Strugnell, W. E., et al. (2004). Eye shape in emmetropia and myopia. *Investigative Ophthalmology and Visual Science, 45*, 3380–3386.

Atchison, D. A., Pritchard, N., White, S. D., & Griffiths, A. M. (2005). Influence of age on peripheral refraction. *Vision Research, 45*(6), 715–720.

Atchison, D. A., & Scott, D. H. (2002). Monochromatic aberrations of human eyes in the horizontal visual field. *Journal of the Optical Society of America A, Optics, Image Science, and Vision, 19*(11), 2180–2184.

Atchison, D. A., Scott, D. H., & Charman, W. N. (2003). Hartmann–Shack technique and refraction across the horizontal visual field. *Journal of the Optical Society of America A, Optics, Image Science, and Vision, 20*(6), 965–973.

Atchison, D. A., Scott, D. H., & Charman, W. N. (2007). Measuring ocular aberrations in the peripheral visual field using Hartmann–Shack aberrometry. *Journal of the Optical Society of America A, Optics, Image Science, and Vision, 24*(9), 2963–2973.

Atchison, D. A., & Smith, G. (1995). Continuous gradient index and shell models of the human lens. *Vision Research, 35*(18), 2529–2538.

Atchison, D. A., & Smith, G. (2005). Chromatic dispersions of the ocular media of human eyes. *Journal of the Optical Society of America A, Optics, Image Science, and Vision, 22*(1), 29–37.

Bedford, R. E., & Wyszecki, G. (1947). Axial chromatic aberration of the human eye. *Journal of the Optical Society of America, 47*(6), 564–565.

Bennett, A. G. (1988). A method of determining the equivalent powers of the eye and its crystalline lens without resort to phakometry. *Ophthalmic & Physiological Optics, 8*(1), 53–59.

Blaker, J. W. (1980). Toward an adaptive model of the human eye. *Journal of the Optical Society of America, 70*(2), 220–223.

Brown, N. (1974). The change in lens curvature with age. *Experimental Eye Research, 19*(2), 175–183.

Calver, R. I., Cox, M. J., & Elliott, D. B. (1999). Effect of aging on the monochromatic aberrations of the human eye. *Journal of the Optical Society of America A, Optics, Image Science, and Vision, 16*(9), 2069–2078.

Campbell, M. C. (1984). Measurement of refractive index in an intact crystalline lens. *Vision Research, 24*(5), 409–415.

Carney, L. G., Mainstone, J. C., & Henderson, B. A. (1997). Corneal topography and myopia. A cross-sectional study. *Investigative Ophthalmology & Visual Science, 38*(2), 311–320.

Cauchy, A. L. (1895). Me'moire sur la dispersion de la lumie're, Nouveaux Exercices de Mathe'matiques, in Oeuvres Comple'tes d'Augustin, 2nd Series, Vol. 10 (Gauthier-Villars et Fils, Paris).

Charman, W. N. (2005). Aberrations and myopia. *Ophthalmic & Physiological Optics, 25*(4), 285–301.

Charman, W. N., & Jennings, J. A. (2006). Longitudinal changes in peripheral refraction with age. *Ophthalmic & Physiological Optics, 26*(5), 447–455.

Cheng, H., Barnett, J. K., Vilupuru, A. S., Marsack, J. D., Kasthurirangan, S., Applegate, R. A., et al. (2004). A population study on changes in wave aberrations with accommodation. *Journal of Vision, 4*(4), 272–280.

Cheng, X., Bradley, A., Hong, X., & Thibos, L. N. (2003). Relationship between refractive error and monochromatic aberrations of the eye. *Optometry and Vision Science, 80*(1), 43–49.

Conrady, A. E. (1960). *Applied optics and optical design Part 2*. New York: Dover. p. 659.

Drasdo, N., & Fowler, C. W. (1974). Non-linear projection of the retinal image in a wide-angle schematic eye. *The British Journal of Ophthalmology, 58*(8), 709–714.

Dubbelman, M., Sicam, V. A., & Van der Heijde, G. L. (2006). The shape of the anterior and posterior surface of the aging human cornea. *Vision Research, 46*(6–7), 993–1001.

Dubbelman, M., & Van der Heijde, G. L. (2001). The shape of the aging human lens: Curvature, equivalent refractive index and the lens paradox. *Vision Research, 41*(14), 1867–1877.

Dubbelman, M., van der Heijde, G. L., & Weeber, H. A. (2001). The thickness of the aging human lens obtained from corrected Scheimpflug images. *Optometry and Vision Science, 78*(6), 411–416.

Dubbelman, M., Van der Heijde, G. L., & Weeber, H. A. (2005). Change in shape of the aging human crystalline lens with accommodation. *Vision Research, 45*(1), 117–132.

Dubbelman, M., Van der Heijde, G. L., Weeber, H. A., & Vrensen, G. F. (2003). Changes in the internal structure of the human crystalline lens with age and accommodation. *Vision Research, 43*(22), 2363–2375.

Dubbelman, M., Weeber, H. A., van der Heijde, R. G., & Volker-Dieben, H. J. (2002). Radius and asphericity of the posterior corneal surface determined by corrected Scheimpflug photography. *Acta Ophthalmologica Scandinavica, 80*(4), 379–383.

Dunne, M. C., Royston, J. M., & Barnes, D. A. (1992). Normal variations of the posterior corneal surface. *Acta ophthalmologica (Copenh), 70*(2), 255–261.

Eghbali, F., Yeung, K. K., & Maloney, R. K. (1995). Topographic determination of corneal asphericity and its lack of effect on the refractive outcome of radial keratotomy. *American Journal of Ophthalmology, 119*(3), 275–280.

Emsley, H. H. (1952) (5th ed.). *Visual optics* (Vol. 1). Butterworths.

Escudero-Sanz, I., & Navarro, R. (1999). Off-axis aberrations of a wide-angle schematic eye model. *Journal of the Optical Society of America A, Optics, Image Science, and Vision, 16*(8), 1881–1891.

Goodman, J. W. (1996). *Introduction to Fourier optics* (2nd ed.). New York: McGraw-Hill.

Goncharov, A. V., & Dainty, C. (2007). Wide-field schematic eye models with gradient-index lens. *Journal of the Optical Society of America A, Optics, Image Science, and Vision, 24*(8), 2157–2174.

Guirao, A., Gonzalez, C., Redondo, M., Geraghty, E., Norrby, S., & Artal, P. (1999). Average optical performance of the human eye as a function of age in a normal population. *Investigative Ophthalmology & Visual Science, 40*(1), 203–213.

Guirao, A., Williams, D. R., & Cox, I. G. (2001). Effect of rotation and translation on the expected benefit of an ideal method to correct the eye's higher-order aberrations. *Journal of the Optical Society of America A, Optics, Image Science, and Vision, 18*(5), 1003–1015.

Gullstrand, A. (1909). Appendices II and IV. In: *Helmholtz's Handbuch der Physiologischen Optik* (Vol. 1, pp. 301–358, 382–415).

Gustafsson, J., Terenius, E., Buchheister, J., & Unsbo, P. (2001). Peripheral astigmatism in emmetropic eyes. *Ophthalmic & Physiological Optics, 21*(5), 393–400.

He, J. C., Gwiazda, J., Thorn, F., & Held, R. (2003). Wave-front aberrations in the anterior corneal surface and the whole eye. *Journal of the Optical Society of America A, Optics, Image Science, and Vision, 20*(7), 1155–1163.

Isabelle, Brunette, Bueno, J. M., Parent, M., Hamam, H., & Simonet, P. (2003). Monochromatic aberrations as a function of age, from childhood to advanced age. *Investigative Ophthalmology & Visual Science, 44*(12), 5438–5446.

Jennings, J. A., & Charman, W. N. (1978). Optical image quality in the peripheral retina. *American Journal of Optometry & Physiological Optics, 55*(8), 582–590.

Jennings, J. A., & Charman, W. N. (1981). Off-axis image quality in the human eye. *Vision Research, 21*(4), 445–455.

Jones, C. E., Atchison, D. A., Meder, R., & Pope, J. M. (2005). Refractive index distribution and optical properties of the isolated human lens measured using magnetic resonance imaging (MRI). *Vision Research, 45*(18), 2352–2366.

Kasprzak, H. T. (2000). New approximation for the whole profile of the human crystalline lens. *Ophthalmic & Physiological Optics, 20*(1), 31–43.

Kelly, J. E., Mihashi, T., & Howland, H. C. (2004). Compensation of corneal horizontal/vertical astigmatism, lateral coma, and spherical aberration by internal optics of the eye. *Journal of Vision, 4*(4), 262–271.

Kooijman, A. C. (1983). Light distribution on the retina of a wide-angle theoretical eye. *Journal of the Optical Society of America, 73*, 1544–1550.

Le Grand, Y., & El Hage, S. G. (1980). *Physiological optics*. Springer-Verlag.

Liang, J., & Williams, D. R. (1997). Aberrations and retinal image quality of the normal human eye. *Journal of the Optical Society of America A, Optics, Image Science, and Vision, 14*(11), 2873–2883.

Liou, H. L., & Brennan, N. A. (1997). Anatomically accurate, finite model eye for optical modeling. *Journal of the Optical Society of America A, Optics, Image Science, and Vision, 14*(8), 1684–1695.

Liu Yong-Ji., Zhao-Qi Wang, Li-Pei Song, & Guo-Guang Mu. (2005). An anatomically accurate eye model with a shell-structure lens. *Optik. 116*, 241–246.

Llorente, L., Diaz-Santana, L., Lara-Saucedo, D., & Marcos, S. (2003). Aberrations of the human eye in visible and near infrared illumination. *Optometry and Vision Science, 80*(1), 26–35.

Lowe, R. F., & Clark, B. A. (1973). Posterior corneal curvature. Correlations in normal eyes and in eyes involved with primary angle-closure glaucoma. *British Journal of Ophthalmology, 57*(7), 464–470.

Lotmar, W. (1971). Theoretical eye model with aspherics. *Journal of the Optical Society of America, 61*, 1522–1529.

Mandelman, T., & Sivak, J. G. (1983). Longitudinal chromatic aberration of the vertebrate eye. *Vision Research, 23*(12), 1555–1559.
Millodot, M. (1981). Effect of ametropia on peripheral refraction. *American Journal of Optometry & Physiological Optics, 58*(9), 691–695.
Mutti, D. O., Sholtz, R. I., Friedman, N. E., & Zadnik, K. (2000). Peripheral refraction and ocular shape in children. *Investigative Ophthalmology & Visual Science, 41*(5), 1022–1030.
Nakao, S., & Ono, T. (1969). Refractive index distribution in the primate crystalline lens and its schematic eye. *Nippon Ganka Kiyo, 20*(5), 533–536.
Navarro, R., Artal, P., & Williams, D. R. (1993). Modulation transfer of the human eye as a function of retinal eccentricity. *Journal of the Optical Society of America A, 10*(2), 201–212.
Navarro, R., Gonzalez, L., & Hernandez-Matamoros, J. L. (2006). On the prediction of optical aberrations by personalized eye models. *Optometry and Vision Science, 83*(6), 371–381.
Navarro, R., Moreno, E., & Dorronsoro, C. (1998). Monochromatic aberrations and point-spread functions of the human eye across the visual field. *Journal of the Optical Society of America A, Optics, Image Science, and Vision, 15*(9), 2522–2529.
Navarro, R., Palos, F., & Gonzalez, L. (2007a). Adaptive model of the gradient index of the human lens. I. Formulation and model of aging ex vivo lenses. *Journal of the Optical Society of America A, Optics, Image Science, and Vision, 24*(8), 2175–2185.
Navarro, R., Palos, F., & Gonzalez, L. M. (2007b). Adaptive model of the gradient index of the human lens. II. Optics of the accommodating aging lens. *Journal of the Optical Society of America A, Optics, Image Science, and Vision, 24*(9), 2911–2920.
Navarro, R., Santamaria, J., & Bescos, J. (1985). Accommodation-dependent model of the human eye with aspherics. *Journal of the Optical Society of America A, 2*(8), 1273–1281.
Norrby, S. (2005). The Dubbelman eye model analysed by ray tracing through aspheric surfaces. *Ophthalmic & Physiological Optics, 25*(2), 153–161.
Palmer, D. A., & Sivak, J. (1981). Crystalline lens dispersion. *Journal of the Optical Society of America, 71*(6), 780–782.
Patel, S., Marshall, J., & Fitzke, F. W. (1993). Shape and radius of posterior corneal surface. *Refractiv and Corneal Surgery, 9*(3), 173–181.
Pierscionek, B. K., & Chan, D. Y. (1989). Refractive index gradient of human lenses. *Optometry and Vision Science, 66*(12), 822–829.
Pierscionek, B. K., Chan, D. Y., Ennis, J. P., Smith, G., & Augusteyn, R. C. (1988). Nondestructive method of constructing three-dimensional gradient index models for crystalline lenses: I. Theory and experiment. *American Journal of Optometry & Physiological Optics, 65*(6), 481–491.
Pomerantzeff, O., Fish, H., Govignon, J., & Schepens, C. L. (1971). Wide angle optical model of the human eye. *Annals of Ophthalmology, 3*(8), 815–819.
Popiolek-Masajada, A., & Kasprzak, H. (2002). Model of the optical system of the human eye during accommodation. *Ophthalmic & Physiological Optics, 22*(3), 201–208.
Popiolek Masajada, A. (1999). Numerical study of the influence of the shell structure of the crystalline lens on the refractive properties of the human eye. *Ophthalmic & Physiological Optics, 19*(1), 41–49.
Porter, J., Guirao, A., Cox, I. G., & Williams, D. R. (2001). Monochromatic aberrations of the human eye in a large population. *Journal of the Optical Society of America A, Optics, Image Science, and Vision, 18*(8), 1793–1803.
Polack, A.(1923), Le chromatisme de l'oeil, Bulletin of Society of Ophthalmology, France 9.
Rabbetts, R. B. (1998). *Bennett–Rabbett's clinical visual optics*. Butterworth-Heinemann publications.
Read, S. A., Collins, M. J., Carney, L. G., & Franklin, R. J. (2006). The topography of the central and peripheral cornea. *Investigative Ophthalmology & Visual Science, 47*(4), 1404–1415.
Rosales, P., Dubbelman, M., Marcos, S., & van der Heijde, R. (2006). Crystalline lens radii of curvature from Purkinje and Scheimpflug imaging. *Journal of Vision, 6*(10), 1057–1067.
Rosales, P., & Marcos, S. (2007). Customized computer models of eyes with intraocular lenses. *Optical Express*(15), 2204–2218.
Salmon, T. O., & van de Pol, C. (2006). Normal-eye Zernike coefficients and root-mean-square wavefront errors. *Journal of the Cataract Refractive Surgery, 32*(12), 2064–2074.
Santamaria, J., Artal, P., & Bescos, J. (1987). Determination of the point-spread function of human eyes using a hybrid optical-digital method. *Journal of the Optical Society of America A, 4*(6), 1109–1114.
Seidemann, A., Schaeffel, F., Guirao, A., Lopez-Gil, N., & Artal, P. (2002). Peripheral refractive errors in myopic, emmetropic, and hyperopic young subjects. *Journal of the Optical Society of America A, Optics, Image Science, and Vision, 19*(12), 2363–2373.
Siedlecki, D., Kasprzak, H., & Pierscionek, B. K. (2004). Schematic eye with a gradient-index lens and aspheric surfaces. *Optical Letters, 29*(11), 1197–1199.
Sivak, J. G., & Mandelman, T. (1982). Chromatic dispersion of the ocular media. *Vision Research, 22*(8), 997–1003.
Sharma, A. K., Kumar, D. V., & Ghatak, A. K. (1982). Tracing rays through graded-index media. *Applied Optics, 21*, 984–987.
Smith, G. (2003). The optical properties of the crystalline lens and their significance. *Clinical & Experimental Optometry, 86*(1), 3–18.
Smith, G., & Atchison, D. A. (2001). The gradient index and spherical aberration of the lens of the human eye. *Ophthalmic & Physiological Optics, 21*(4), 317–326.
Smith, G., Atchison, D. A., & Pierscionek, B. K. (1992). Modeling the power of the aging human eye. *Journal of the Optical Society of America A, 9*(12), 2111–2117.
Smith, G., & Garner, L. F. (1996). Determination of the radius of curvature of the anterior lens surface from the Purkinje images. *Ophthalmic & Physiological Optics, 16*(2), 135–143.
Smith, G., Pierscionek, B. K., & Atchison, D. A. (1991). The optical modelling of the human lens. *Ophthalmic & Physiological Optics, 11*(4), 359–369.
Stiles, W. S., & Crawford, B. H. (1993). The luminance efficiency of rays entering the eye pupil at different points. *Proceedings of the Royal Society: Part B, 112*, 428–450.
Thibos, L. N., Bradley, A., & Hong, X. (2002). A statistical model of the aberration structure of normal, well-corrected eyes. *Ophthalmic & Physiological Optics, 22*(5), 427–433.
Thibos, L. N., Hong, X., Bradley, A., & Cheng, X. (2002). Statistical variation of aberration structure and image quality in a normal population of healthy eyes. *Journal of the Optical Society of America A, Optics, Image Science, and Vision, 19*(12), 2329–2348.
Thibos, L. N., Ye, M., Zhang, X., & Bradley, A. (1992). The chromatic eye: A new reduced-eye model of ocular chromatic aberration in humans. *Applied Optics, 31*, 3594–3600.
Vazquez, D., Acosta, E., Smith, G., & Garner, L. (2006). Tomographic method for measurement of the gradient refractive index of the crystalline lens. II. The rotationally symmetrical lens. *Journal of the Optical Society of America A, Optics, Image Science, and Vision, 23*(10), 2551–2565.
Wang, L., & Koch, D. D. (2003). Ocular higher-order aberrations in individuals screened for refractive surgery. *Journal of Cataract Refractive Surgery, 29*(10), 1896–1903.
Williams, D. R., Artal, P., Navarro, R., McMahon, M. J., & Brainard, D. H. (1996). Off-axis optical quality and retinal sampling in the human eye. *Vision Research, 36*(8), 1103–1114.
Zadnik, K., Manny, R. E., Yu, J. A., Mitchell, G. L., Cotter, S. A., Quiralte, J. C., et al. (2003). Ocular component data in schoolchildren as a function of age and gender. *Optometry and Vision Science, 80*(3), 226–236.
ZEMAX. (2007). Software for Optical System Design. Bellevue, WA, USA.